Electron and hole transport in the APFO3:$PC_{61}BM$ organic photovoltaic blends

L. G. WANG*, C. G. WANG, Y. L. LIANG, L. ZHANG, J. Y. LIU*
School of Electrical Engineering and Automation, Henan Key Laboratory of Intelligent Detection and Control of Coal Mine Equipment, Henan Polytechnic University, Jiaozuo, 454003, People's Republic of China

In this paper, the electron and hole transport properties, and the possible presence of spatially correlated disorder in the APFO3:$PC_{61}BM$ organic blends are investigated. The temperature dependent current density-voltage ($J-V$) characteristics of the hole-only and electron-only devices based on the APFO3:$PC_{61}BM$ blends can be consistently described by using the improved extended Gaussian disorder model (IEGDM) and the extended correlated disorder model (ECDM), within which includes the carrier density dependence of the mobility in the Gaussian density of states and assuming either random or spatially correlated site energies. In contrast to the ECDM, the IEGDM provides a better description for both hole and electron transport. Based on the comparison of the intersite distance and fit quality of $J-V$ curves between the IEGDM and ECDM, we argue that the analysis provides evidence for the absence of correlated disorder in the APFO3:$PC_{61}BM$ blends. Furthermore, it is found that energetic disorder is larger for holes than for electrons, and electron transport is intrinsically superior to hole transport.

(Received July 26, 2022; accepted April 5, 2023)

Keywords: Electron transport, Hole transport, Energetic disorder, Intersite distance

1. Introduction

Organic semiconductors have promising applications in organic optoelectronic devices, such as solar cells [1-4], which typically consist of a disordered mixture of donor (D) and acceptor (A) materials. Making an optimal combination of an electron donating material and an electron accepting material in a bulk heterojunction (BHJ) for efficient organic photovoltaic devices (OPV) is an incredibly complicated and multifaceted endeavor [5, 6], despite the seemingly simple approach of material mixing. Focus areas in the development of new materials and devices have since long been the selection of energy levels and control over the multiscale microstructure [7, 8]. In order to obtain a larger open circuit voltage, the donor material should have a lower energy bandgap, so that the absorption spectrum of the material can reach the best matching value with the solar spectrum. One of the most promising low bandgap organic semiconductors to date is polyfluorene copolymer (Poly[2,7-(9-di-octyl-fluorene)-alt -5,5-(4',7'-di-2-thienyl-2',1',3'-benzothiadiazole)], APFO3), which is composed of the electron-donor unit (fluorine group) and the electron-acceptor units (benzothiadiazole and two thiophene units). Its absorption bandedge has reached ~700 nm in the solution and its carrier mobility is also excellent, which makes it suitable for photovoltaic application [9]. A significant part of the efforts made in this field has been the optimization of the fabrication of solar cells based on APFO3:$PC_{61}BM$ (methanofullerene [6,6]-phenyl C_{61}-butyric acid methyl ester) blends [10, 11]. However, charge transport and energetic disorder in APFO3:$PC_{61}BM$ blends have been largely ignored, as research has focused more on photophysical properties of the mixing materials. Thorough understanding of the charge transport properties and energetic disorder is important for developing more stable and efficient APFO3:$PC_{61}BM$-based organic photovoltaic devices.

Charge transport in organic semiconductors is usually characterized by hopping transport between states that have a certain distribution in energy. This energetic disorder stems from the morphological ordering of the molecules and is frequently assumed to have a Gaussian distribution [12]. Current theoretical research pursues to predict the mobility and energetic disorder by starting from microscopic simulations of the morphology, paving the way to predictive modeling of organic materials and devices [13-15]. The effects of disorder on the mobility are frequently described within the Gaussian disorder model (GDM) [12] or the correlated disorder model (CDM) [16], assuming a Gaussian density of state (DOS) with random and spatially correlated energetic disorder, respectively. Later, it was realized that, apart from the dependence of the mobility on the temperature and electric field, there is a strong dependence on the carrier concentration, giving rise to the extended versions of the GDM and CDM, the EGDM and ECDM [17, 18], respectively. For small but

realistic electric fields, the field dependence of the mobility is within the ECDM much stronger than within the EGDM. On the other hand, the charge carrier density dependence is for the ECDM slightly weaker. However, the EGDM and ECDM, only having a non-Arrhenius temperature dependence $\ln(\mu) \propto 1/T^2$, cannot well describe charge transport at high carrier densities [19]. To better describe the charge transport properties, we proposed an improved version of the EGDM within which the temperature dependence of the mobility based on both the non-Arrhenius temperature dependence and Arrhenius temperature dependence $\ln(\mu) \propto 1/T$, leading to the IEGDM [20]. Being able to make a distinction between the EGDM and ECDM, to determine the type of disorder and to accurately extract the materials parameters that determine the mobility in disordered organic semiconductors is of great importance to the rational design of organic photovoltaic devices. Analyses of measured current density versus voltage ($J-V$) curves of sandwich-type devices based on several polymers have been successfully carried out using the EGDM [21, 22], whereas for several small-molecule materials, a more consistent analysis was obtained by using the ECDM [23, 24]. These studies revealed that equally good descriptions of the steady-state $J-V$ curves could be obtained from both models, but that a distinction could be made on the basis of the effective hopping site densities obtained. For polymers only the EGDM led to a hopping site density close the actual molecular site density, whereas for the same reason the ECDM was found to be most appropriate for small-molecule materials. The question now arises whether it would also be possible to describe the $J-V$ curves of single-carrier devices based on polymer:fullerene blends using the EGDM or ECDM, and whether it would again be possible to make a distinction between both models on the basis of the site density obtained.

In this paper, we will investigate whether such an extensive analysis can be given for electron and hole transport in sandwich-type single-carrier devices based on the APFO3:$PC_{61}BM$ blends. From an analysis of the temperature dependence of the $J-V$ characteristics of APFO3:$PC_{61}BM$ electron-only and hole-only devices, it is found that good descriptions can be obtained within the IEGDM and ECDM. However, the more realistic values of the intersite distance for electron-only and hole-only devices are obtained within the IEGDM than within the ECDM. This is an indication that in the APFO3:$PC_{61}BM$ blends correlations between the site energies are absent or play a minor role.

2. Models and methods

A commonly employed mobility model has been developed by Pasveer et al. on basis of numerical transport simulations accounting for hopping on a simple cubic lattice with uncorrelated Gaussian disorder [17]. For historical reasons this model is often referred to as the EGDM. However, the EGDM only with a non-Arrhenius temperature dependence, cannot well describe charge transport at high carrier densities. To better describe charge transport, we proposed an improved version of the EGDM within which the temperature dependence of the mobility based on both the non-Arrhenius temperature dependence and Arrhenius temperature dependence, leading to the IEGDM [20]. Previously, the IEGDM has been successfully applied to describe charge transport in disordered organic semiconductors [25-27]. In the IEGDM, the dependence of the zero-field mobility on the carrier density p and temperature T is given by

$$\mu(T,p) = \mu_0(T)\exp[\frac{1}{2}\left(\hat{\sigma}^2 - \hat{\sigma}\right)\left(2pa^3\right)^{\delta}], \quad (1a)$$

$$\mu_0(T) = \mu_0 c_1 \exp(c_2\hat{\sigma} - c_3\hat{\sigma}^2), \quad (1b)$$

$$\delta \equiv 2\frac{\ln(\hat{\sigma}^2 - \hat{\sigma}) - \ln(\ln 4)}{\hat{\sigma}^2}, \quad \mu_0 \equiv \frac{a^2\nu_0 e}{\sigma}, \quad (1c)$$

with $c_1 = 0.48 \times 10^{-9}$, $c_2 = 0.80$, and $c_3 = 0.52$. Where $\mu_0(T)$ is the mobility in the limit of zero carrier density and electric field, $\hat{\sigma} \equiv \sigma / k_B T$ is the dimensionless disorder parameter, σ is the width of the Gaussian density of states (DOS), a is the lattice constant (intersite distance), e is the charge of the carriers, and ν_0 is the attempt frequency. The field dependence of the mobility is included via

$$\mu(T,p,E) = \mu(T,p)^{g(T,E)}\exp[c_4\left(g(T,E)-1\right)], \quad (2)$$

$$g(T,E) = [1 + c_5(Eea/\sigma)^2]^{-1/2}, \quad (3)$$

where $g(T,E)$ is a weak density dependent function, c_4 and c_5 are weak density dependent parameters, given by

$$c_4 = d_1 + d_2\ln(pa^3) \quad (4a)$$

$$c_5 = 1.16 + 0.09\ln(pa^3) \quad (4b)$$

$$d_1 = 28.7 - 36.3\hat{\sigma}^{-1} + 42.5\hat{\sigma}^{-2} \quad (5a)$$

$$d_2 = -0.38 + 0.19\hat{\sigma} + 0.03\hat{\sigma}^2 \quad (5b)$$

In addition to uncorrelated energetic disorder, the presence of molecular dipoles may give rise to spatial correlations in the energy distribution of the sites. Bouhassoune et al. employed the same methodology as in the EGDM, but for an energy landscape with Gaussian disorder that result from randomly oriented dipole moments of equal magnitude on all lattice sites, leading to the ECDM [18]. The mobility can be described as

follows:

$$\mu(T,p,E)=[(\mu_{low}(T,p,E))^{q(\hat{\sigma})}+(\mu_{high}(p,E))^{q(\hat{\sigma})}]^{1/q(\hat{\sigma})}, \tag{6}$$

$$q(\hat{\sigma})=2.4/(1-\hat{\sigma}), \tag{7}$$

with $\mu_{low}(T,p,E)$ the mobility in the low-field limit, and $\mu_{high}(p,E)$ the mobility in the high-field limit.

$$\mu_{low}(T,p,E)=\mu_0(T)g(T,p)f(T,E,p) \tag{8}$$

where $g(T,p)$ and $f(T,E,p)$ are the dimensionless mobility enhancement functions. These functions can be written as follows:

$$\mu_0(T)=1.0\times10^{-9}\mu_0\exp(-0.29\hat{\sigma}^2), \tag{9}$$

$$g(T,p)=\begin{cases}\exp[(0.25\hat{\sigma}^2+0.7\hat{\sigma})(2pa^3)^{\delta}], pa^3<0.025\\ g(T,0.025a^{-3}), pa^3\geq0.025\end{cases}, \tag{10}$$

$$\delta\equiv2.3\frac{\ln(0.5\hat{\sigma}^2+1.4\hat{\sigma})-0.327}{\hat{\sigma}^2}, \tag{11}$$

$$f(T,E_{red},p)=\exp[h(E_{red})(1.05-1.2(pa^3)^{r(\hat{\sigma})})(\hat{\sigma}^{3/2}-2)(\sqrt{1+2E_{red}}-1)] \tag{12}$$

$$h(E_{red})=1,\ \ r(\hat{\sigma})=0.7\hat{\sigma}^{-0.7}, \tag{13}$$

within the very low-field, $0\leq E_{red}<0.16\equiv E^*_{red}$, $h(E_{red})$ can be written as

$$h(E_{red})=\begin{cases}\frac{4}{3}\frac{E_{red}}{E^*_{red}}, (E_{red}\leq E^*_{red}/2)\\ \left[1-\frac{4}{3}\left(\frac{E_{red}}{E^*_{red}}-1\right)^2\right], (E^*_{red}/2\leq E_{red}\leq E^*_{red})\end{cases} \tag{14}$$

$$\mu_{high}(p,E)=\frac{2.06\times10^{-9}}{E_{red}}\mu_0(1-pa^3)\cdot \tag{15}$$

Using the above model and the following coupled equations, the $J-V$ characteristics of organic electron devices can be exactly calculated by employing a particular uneven discretization method introduced in our previous papers [28, 29].

$$J=p(x)e\mu(T,p(x),E(x))E(x), \tag{16a}$$

$$\frac{dE}{dx}=\frac{e}{\varepsilon_0\varepsilon_r}p(x), \tag{16b}$$

$$V=\int_0^L E(x)dx, \tag{16c}$$

where x is the distance from the injecting electrode, ε_0 is the vacuum permeability, ε_r is the relative dielectric constant of the organic semiconductors, and L is the organic semiconductor layer thickness sandwiched between two electrodes.

3. Results and discussion

To explore the charge transport properties in more detail and evaluate the energetic disorder, we investigate the temperature dependent space-charge limited current for hole-only and electron-only devices based on the APFO3:$PC_{61}BM$ blends. Fig. 1 and Fig. 2 show the $J-V$ curves of a hole-only device with a thickness of 99 nm at different temperatures. The solid lines in Fig.1 and Fig.2 represent the numerical calculation results of IEGDM and ECDM combined with the coupled equations (Eqs.(16)), and the symbols are the experimental measurements of the $J-V$ characteristics from Ref. [11]. It can be seen from the figures that the numerical simulations based on both the IEGDM and ECDM models are in close agreement with the experimental data. In contrast to the ECDM, the IEGDM provides a better description for hole current. The IEGDM and ECDM are the mobility functions that describe the temperature-, density-, and field-dependence of the mobility based on three input parameters, viz. the width of the Gaussian energetic disorder σ, the lattice constant a, and a mobility prefactor μ_0. The μ_0 is a temperature independent parameter that only influences the magnitude of the mobility, σ mainly controls the temperature and charge concentration dependence of the mobility, and a predominantly affects the field dependence of the mobility. By fitting the IEGDM and ECDM to the charge transport measurements, these parameters can be reliably determined. The three parameters in the IEGDM and ECDM are a=1.11 nm, σ=0.089 eV, μ_0=48 cm^2/Vs, and a=0.07 nm, σ=0.088 eV, μ_0=35 cm^2/Vs, respectively. It is found that the best-fit values of the intersite distance a as obtained from the IEGDM and ECDM are quite different. The value of a obtained from the ECDM can be considered as unrealistically small (significantly lower than the typical value of organic semiconductors), in view of the fact that in polymer APFO3 the use of side-chain architecture is expected to give rise to a larger typical distance between neighboring polymer chains in the APFO3:$PC_{61}BM$ blends [9]. Furthermore, intra-chain hopping between the rather long segments is also expected to be associated with larger a. However, the value of a obtained from the IEGDM is very close to the typical value of organic semiconductors, and smaller than the value obtained by Felekidis et al. for the APFO3:$PC_{61}BM$ blends [10]. These results indicate that there is no correlation between the transport site energies in the APFO3:$PC_{61}BM$ blends. The comparison between the values obtained for σ and μ_0 does not change this point of view. For disordered organic semiconductors, the width of the DOS is typically observed to fall in the range 0.06-0.15 eV. Clearly, the optimal value of σ obtained

from the IEGDM (0.089 eV) is almost equal to that from the ECDM (0.088 eV) , and both are physically realistic.

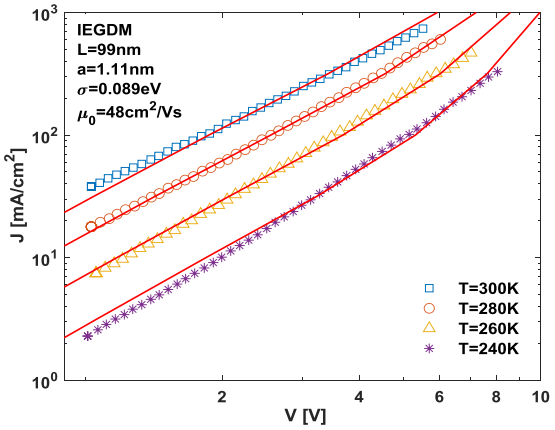

Fig. 1. Temperature dependent J-V characteristics of a hole-only device based on the APFO3:$PC_{61}BM$ blends with a layer thickness of 99 nm. Symbols are the experimental results from Ref. [11]. Lines are the numerically calculated results based on the IEGDM (color online)

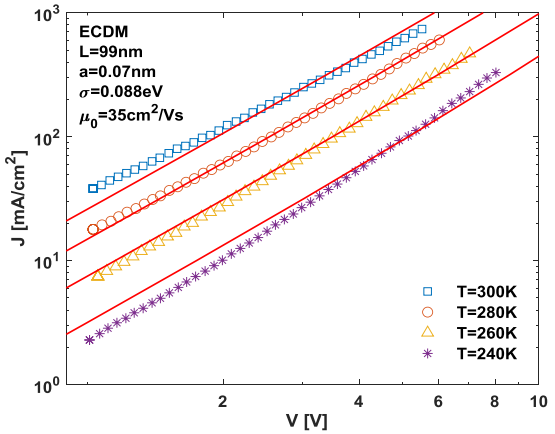

Fig. 2. Temperature dependent J-V characteristics of a hole-only device based on the APFO3:$PC_{61}BM$ blends with a layer thickness of 99 nm. Symbols are the experimental results from Ref. [11]. Lines are the numerically calculated results based on the ECDM (color online)

Having characterized hole transport, we will now focus on electron transport. From a theoretical perspective, the intrinsic electron and hole transport are comparable in many organic semiconductors [30], which would also be expected to hold for polymer:fullerene blends. However, experimentally, hole transport usually shows trap-free behavior, while electron transport is severely hindered by charge trapping [31]. When the trap level becomes filled a transition to a higher, trap-free space-charge limited current occurs. In order to ensure that the intrinsic charge transport properties of the investigated material are actually probed, the fitting range has to be shifted to voltages where all the traps have been filled. Fig.3 and Fig.4 show the $J-V$ curves of an electron-only device with a thickness of 183 nm at different temperatures. The solid lines in Fig.3 and Fig.4 represent the numerical calculation results of IEGDM and ECDM combined with the coupled equations (Eqs.(16)), and the symbols are the experimental measurements of the $J-V$ characteristics from Ref. [11]. It is clear that the numerical simulations based on both the IEGDM and ECDM models are in close agreement with the experimental data when the voltage is greater than 4V. At high voltages, a transition to a less steep slope of the $J-V$ characteristics is observed, which indicates that the current approaches the trap-filled limit. The three parameters in the IEGDM and ECDM are a =1.42 nm, σ =0.0645 eV, μ_0 =110 cm^2/Vs, and a =0.36 nm, σ =0.0715 eV, μ_0 =165 cm^2/Vs, respectively. It is also found that the best-fit values of the intersite distance a as obtained from the IEGDM and ECDM are quite different. The value of a obtained from the ECDM can be considered as unrealistically small, whereas the value of a from the IEGDM is realistic. In addition, the values of σ and μ_0 from the IEGDM are closer to that obtained from the ECDM. These results further indicate that there is no correlation between transport site energy in the APFO3:$PC_{61}BM$ blends.

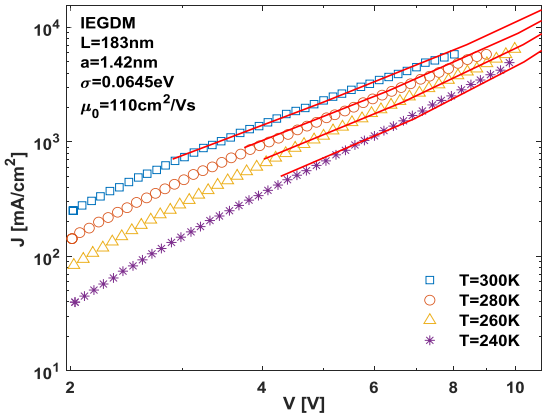

Fig. 3. Temperature dependent J-V characteristics of an electron-only device based on the APFO3:$PC_{61}BM$ blends with a layer thickness of 183 nm. Symbols are the experimental results from Ref. [11]. Lines are the numerically calculated results based on the IEGDM (color online)

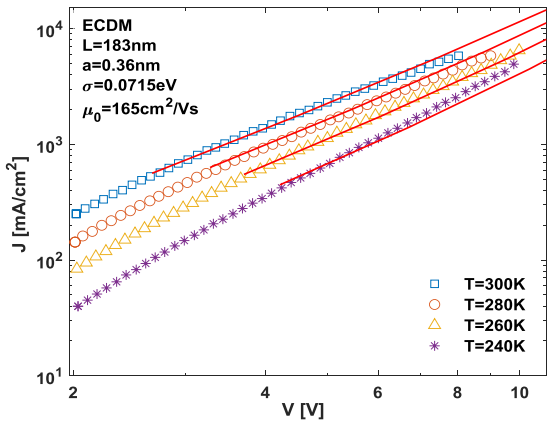

Fig. 4. Temperature dependent J-V characteristics of an electron-only device based on the APFO3:$PC_{61}BM$ blends with a layer thickness of 183 nm. Symbols are the experimental results from Ref. [11]. Lines are the numerically calculated results based on the ECDM (color online)

It can be seen from Figs. 1-4 that good descriptions of the temperature dependent $J-V$ characteristics of hole-only and electron-only devices based on the APFO3:$PC_{61}BM$ blends can be obtained within both the IEGDM and ECDM. Compared with the ECDM, the IEGDM provides a better fit quality for both hole and electron transport. The intersite distance a as obtained from the IEGDM and ECDM are quite different. The value of a from the IEGDM is very close to the typical value of organic semiconductors, whereas the value of a from the ECDM may be considered as unrealistically small. These results show that the energies of the sites in between which hopping takes place are uncorrelated in the APFO3:$PC_{61}BM$ blends. The width of the Gaussian distribution σ found for electron transport is smaller than that for hole transport, indicating a lower degree of energetic disorder for electron transport in the APFO3:$PC_{61}BM$ blends. The observation of weak disorder is in agreement with the higher electron current as displayed in Fig.3 and Fig.4. As a result, it is evident that electron transport is better than hole transport in the APFO3:$PC_{61}BM$ blends. This further indicates that the intrinsic electron and hole transport are comparable for most organic semiconductors.

4. Summary and conclusions

In conclusion, charge transport and the possible presence of spatially correlated disorder in the APFO3:$PC_{61}BM$ blends are investigated. It is found that the temperature dependent $J-V$ characteristics of the hole-only and electron-only devices based on the APFO3:$PC_{61}BM$ blends can be well described using both the IEGDM and ECDM. However, the intersite distance obtained from the IEGDM is more realistic than the value obtained from the ECDM, which indicates that the correlations between the transport site energies in the APFO3:$PC_{61}BM$ blends are absent. Furthermore, it is found that energetic disorder is larger for holes than for electrons, and electron transport is superior to hole transport in the APFO3:$PC_{61}BM$ blends.

Acknowledgements

This work is supported by the Key Scientific Research Project of Colleges and Universities in Henan Province Grant No. 21B470005, the Fundamental Research Funds for the Universities of Henan Province Grant No. NSFRF200304 and No. NSFRF210424, the Science and Technology Project of Henan Province Grant No. 202102210295, the Young Key Teacher Program of Henan Polytechnic University Grant No. 2019XQG-17, and the Doctoral Scientific Research Foundation of Henan Polytechnic University Grant No. B2014-022 and No. B2017-20.

References

[1] L. Meng, Y. Zhang, X. Wan, C. Li, X. Zhang, Y. Wang, X. Ke, Z. Xiao, L. Ding, R. Xia, H. Yip, Y. Cao, Y. Chen, Science **361**, 1094 (2018).
[2] X. Che, Y. Li, Y. Qu, S. R. Forrest, Nat. Energy **3**, 422 (2018).
[3] J. Yuan, Y. Zhang, L. Zhou, G. Zhang, H. L. Yip, T. Lau, X. Lu, C. Zhu, H. Peng, P. A. Johnson, M. Leclerc, Y. Cao, J. Ulanski, Y. Li, Y. Zou, Joule **3**, 1140 (2019).
[4] J. Wu, H. Cha, T. Du, Y. Dong, W. Xu, C. Lin, J. R. Durrant, Adv. Mater. **34**, 2101833 (2021).
[5] N. Felekidis, A. Melianas, M. Kemerink, ACS Appl. Mater. Interfaces **9**, 37070 (2017).
[6] N. Felekidis, A. Melianas, M. Kemerink, J. Phys. Chem. Lett. **11**, 3563 (2020).
[7] R. E. M. Willems, C. H. L. Weijtens, X. de Vries, R. Coehoorn, R. A. J. Janssen, Adv. Energy Mater. **9**, 1803677 (2019).
[8] A. G. Ricciardulli, P. W. M. Blom, Adv. Mater. Technol. **5**, 1900972 (2020).
[9] A. Gadisa, F. L. Zhang, D. Sharma, M. Svensson, M. R. Andersson, O. Inganas, Thin Solid Films **515**, 3126 (2007).
[10] N. Felekidis, A. Melianas, M. Kemerink, Org. Electron. **61**, 318 (2018).
[11] A. Melianas, N. Felekidis, Y. Puttisong, S. C. J. Meskers, O. Inganäs, W. M. Chen, M. Kemerink, Applied Physical Sciences **116**, 23416 (2019).
[12] H. Bässler, Phys. Status Solidi B **175**, 15 (1993).
[13] F. May, B. Baumeier, C. Lennartz, D. Andrienko, Phys. Rev. Lett. **109**, 136401 (2012).
[14] A. Masse, P. Friederich, F. Symalla, F. Liu,

R. Nitsche, R. Coehoorn, W. Wenzel, P. A. Bobbert, Phys. Rev. B **93**, 195209 (2016).
[15] W. Liu, N. B. Kotadiya, P. W. M. Blom, G. J. A. H. Wetzelaer, D. Andrienko, Adv. Mater. Technol. **6**, 2000120 (2021).
[16] Y. N. Gartstein, E. M. Conwell, Chem. Phys. Lett. **245**, 351 (1995).
[17] W. F. Pasveer, J. Cottaar, C. Tanase, R. Coehoorn, P. A. Bobbert, P. W. M. Blom, D. M. de Leeuw, M. A. J. Michels, Phys. Rev. Lett. **94**, 206601 (2005).
[18] M. Bouhassoune, S. L. M. van Mensfoort, P. A. Bobbert, R. Coehoorn, Org. Electron. **10**, 437 (2009).
[19] N. I. Craciun, J. Wildeman, P. W. M. Blom, Phys. Rev. Lett. **100**, 056601 (2008).
[20] L. G. Wang, H. W. Zhang, X. L. Tang, C. H. Mu, Eur. Phys. J. B **74**, 1 (2010).
[21] R. J. de Vries, S. L. M. van Mensfoort, V. Shabro, S. I. E. Vulto, R. A. J. Janssen, R. Coehoorn, Appl. Phys. Lett. **94**, 163307 (2009).
[22] X. L. Wang, L. Zhang, L. A. Kang, L. G. Wang, Optoelectron. Adv. Mat. **14**(7-8), 372 (2020).
[23] S. L. M. van Mensfoort, V. Shabro, R. J. de Vries, R. A. J. Janssen, R. Coehoorn, J. Appl. Phys. **107**, 113710 (2010).
[24] S. L. M. van Mensfoort, R. J. de Vries, V. Shabro, H. P. Loebl, R. A. J. Janssen, R. Coehoorn, Org. Electron. **11**, 1408 (2010).
[25] I. Katsouras, A. Najafi, K. Asadi, A. J. Kronemeijer, A. J. Oostra, L. J. A. Koster, D. M. de Leeuw, P. W. M. Blom, Org. Electron. **14**, 1591 (2013).
[26] L. G. Wang, M. L. Liu, J. J. Zhu, L. F. Cheng, Optoelectron. Adv. Mat. **11**, 202 (2017).
[27] B. B. Cui, L. G. Wang, M. L. Liu, Y. Guo, W. Zhang, Optoelectron. Adv. Mat. **12**(9-10), 512 (2018).
[28] L. G. Wang, H. W. Zhang, X. L. Tang, Y. Q. Song, Optoelectron. Adv. Mat. **5**(3), 263 (2011).
[29] M. L. Liu, L. G. Wang, J. Optoelectron. Adv. M. **19**(5-6), 406 (2017).
[30] V. Coropceanu, J. Cornil, D. A. da Silva Filho, Y. Olivier, R. Silbey, J. L. Bredas, Chem. Rev. **107**, 926 (2007).
[31] H. T. Nicolai, M. Kuik, G. A. H. Wetzelaer, B. de Boer, C. Campbell, C. Risko, J. L. Bredas, P. W. M. Blom, Nat. Mater. **11**, 882 (2012).

*Corresponding author: wangliguo@hpu.edu.cn; liujy@hpu.edu.cn